Terr. Atmos. Ocean. Sci., Vol. 23, No. 6, 725-732, December 2012 doi: 10.3319/TAO.2012.06.19.01(T)

NOTES AND CORRESPONDENCE

Sensitivity of Deep-Towed Marine Electrical Resistivity Imaging Using Two-Dimensional Inversion: A Case Study on Methane Hydrate

Chih-Wen Chiang[1,*], Tada-nori Goto[2], Hitoshi Mikada[2], Chien-Chih Chen[1], and Shu-Kun Hsu[1]

[1] *Department of Earth Sciences, National Central University, Jhongli, Taiwan*
[2] *Department of Civil and Earth Resources Engineering, Kyoto University, Kyoto, Japan*

Received 28 December 2011, accepted 19 June 2012

ABSTRACT

Uncertain physical properties of methane hydrate (MH) above a bottom simulating reflector should be estimated for detecting MH-bearing formations. In contrast to general marine sediments, MH-bearing formations have a relatively high electrical resistivity. Therefore, marine electrical resistivity imaging (MERI) is a well-suited method for MH exploration. The authors conducted sensitivity testing of sub-seafloor MH exploration using a two-dimensional (2D) inversion algorithm with the Wenner, Pole-Dipole (PD) and Dipole-Dipole (DD) arrays. The results of the Wenner electrode array show the poorest resolution in comparison to the PD and DD arrays. The results of the study indicate that MERI is an effective geophysical method for exploring the sub-seafloor electrical structure and specifically for delineating resistive anomalies that may be present because of MH-bearing formations at a shallow depth beneath the seafloor.

Key words: Methane hydrate, Gas hydrate, Deep-towed marine electrical resistivity imaging, 2D inversion, DC survey

Citation: Chiang, C. W., T. Goto, H. Mikada, C. C. Chen, and S. K. Hsu, 2012: Sensitivity of deep-towed marine electrical resistivity imaging using two-dimensional inversion: A case study on methane hydrate. Terr. Atmos. Ocean. Sci., 23, 725-732, doi: 10.3319/TAO.2012.06.19.01(T)

1. INTRODUCTION

MH is thought to be widely distributed within the continental margins and permafrost regions of the Earth (Lin et al. 2006). These deposits were formed in sub-seafloor sediments at relatively high pressure, low temperature conditions and have the potential to become a significant energy resource in the future (e.g., Kvenvolden 1988; Johnson and Max 2006; Lin et al. 2006). Gaseous methane is a greenhouse gas released potentially at the sub-seafloor level through the dissociation of gas hydrate along fault ruptures (Schwalenberg et al. 2010) and through other mechanisms. Therefore, studying MH is a possible solution for depleted energy resources and the impact of current energy resources on climate change.

Over the past few decades, active offshore seismic surveys have associated bottom simulating reflectors (BSRs) with the occurrence of MH-bearing formations (Shipley et al. 1979; Hyndman et al. 1992). The BSRs correspond to the base of the phase boundary that exists between free gases and the solid hydrates indicative of an MH deposit. BSRs provide constraint on the solid-gas boundary that occurs at the base of MH deposits. However, approximately 90% of potential fields explored by BSRs are filled with saline water (Thirud 2002). In addition, MH deposits have been located in areas which do not show a BSR indicator (Paull et al. 2000).

Typically, MH resistivity is within the range 3 - 10 ohm-m in-field (Schwalenberg et al. 2010). In contrast, the resistivity of marine sediments generally ranges from 0.8 to 1.5 ohm-m, and the resistivity of seawater (although dependent on salinity and temperature variations) is generally within the range of 0.286 to 0.33 ohm-m. Therefore, the large resistivity contrast that exists between these features may provide an excellent opportunity to image electrical resistivity anomalies beneath the seafloor (Von Herzen et al. 1996; Goto et al. 2008; Chiang et al. 2011). However,

* *Corresponding author*
E-mail: devenchiang@gmail.com

inversion studies concerning sensitivity have not yet been completed, and past studies have been based on one-dimensional data-processing methods (Francis 1985; Von Herzen et al. 1996; Goto et al. 2008; Schwalenberg et al. 2010), which are unable to account for lateral variations in the sub-seafloor structure.

To investigate the sensitivity of the MERI method, three traditional land electrical resistivity imaging (LERI) arrays: Wenner, PD, and DD were evaluated using a 2D inversion algorithm. A conventional non-linear least-squares 2D inversion algorithm (Griffith and Barker 1993) was used to test the resolution of the MERI method for various electrode arrangements. Based on the inversion results of the numerical study, the effectiveness of using deep-towed MERI to image a buried MH zone can be well understood and further determine the optimum array configuration.

2. GEOMETRIC FACTOR OF MERI

General LERI prospecting is widely applied to investigate electrical resistivity structures through the controlled injection of a current into the subsurface and measurement of the potential difference between pairs of electrodes at the surface. The apparent resistivity is then determined using the following equation:

$$\rho_a = K\frac{V}{I} \tag{1}$$

where ρ_a: apparent resistivity, K: geometric factor, V: potential, and I: electrical current. For LERI applications, the geometric factor is determined for a half-space defined by the boundary between (insulating) air and the conductive ground (Fig. 1). The Wenner, DD, and PD array geometric factors for LERI are shown in the following equations:

$$K = 2\pi a \tag{2a}$$

$$K = \pi n(n+1)(n+2)a \tag{2b}$$

$$K = 2\pi n(n+1)a \tag{2c}$$

In contrast, in MERI applications the geometric factor is defined for quasi-space encompassing both the conductive seawater and sub-seafloor (Fig. 1). The Wenner DD, and PD array geometric factors for MERI are derived from the following equations:

$$K = 4\pi a \tag{3a}$$

$$K = 2\pi n(n+1)(n+2)a \tag{3b}$$

$$K = 4\pi n(n+1)a \tag{3c}$$

In these equations, "a" represents the spacing of receiver electrodes and "n" represents current sources and receiver offset. The three configurations of MERI are shown in Fig. 2.

3. TWO-DIMENSIONAL INVERSION

Previous MERI experiments (Francis 1985; Von Herzen et al. 1996; Goto et al. 2008; Chiang et al. 2011) did not check their imaging abilities with an inversion algorithm which realistically accounted for noise effect; thus, this study used conventional Wenner, PD, and DD arrays to ensure that this effect was accounted for. The synthetic

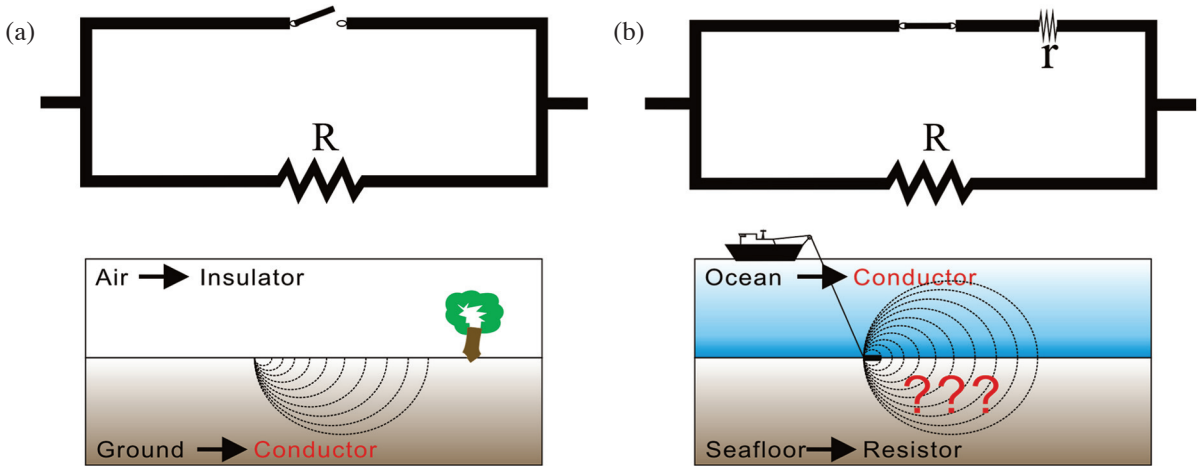

Fig. 1. Diagram of the difference between LERI and MERI exploration. R: large resistor; r: small resistor. The electric currents were all injected into the ground for the LERI (a), while the electrical current passed to both resistors for the MERI (b).

model is shown in Fig. 3. The resistivity of the sedimentary layer and the MH are each changed to 1 ohm-m in 50 m in thickness, 10 ohm-m in 30 m in thickness, and 195 m in horizontal width. The electrode dipole length ("a" in Fig. 2) can be sequentially changed from 20 to 200 m in 20 m steps (11 receiver electrodes). For the source-receiver offset ("n" in Fig. 2), a long offset generates a small S/N ratio (Loke and Barker 1996). In general, the DD array on LERI was limited within a factor of 6 due to the concern of S/N ratio (Loke and Barker 1996), yet the Wenner array does not have such "n" factor limitation. Therefore, the "n" factor has been restricted from 1 to 3 in this study. The shortest cable length is 60 m for the DD and Wenner arrays, and 40 m for the PD array (when n = 1 and a = 20 m); the longest cable length is extended to 1000 m for the DD array, 800 m for the PD array, and 600 m for the Wenner array (where n = 3 and a = 200 m). The induced current is set 16 amperes for the Wenner and the DD arrays and 8 amperes for the PD array. The lower current amplitude selected for the PD array is due to excess heat generated in the cables for this array configuration (Goto 2009, personal communication). To test the sensitivity of the various electrode arrays, 30 μV of Gaussian noise was added to the synthetic modeling results, based on a field experiment (Goto et al. 2008; Goto 2009, personal communication). The apparent resistivities for Wenner, PD, and DD array with and without noise are shown in Figs. 4 to 6 as pseudo-sections.

Figure 4b shows that both the shape and magnitude of the apparent resistivity are relatively insensitive to the presence of noise for the Wenner array calculated from Eq. (3a). In contrast, the PD array of the pseudo-sections is strongly influenced by the presence of noise with the varying source-receiver offsets (n = 1 to 3), as shown in Figs. 5b, d, and f, respectively. The non-symmetric pseudo-sections "without noise" appear at the all source-receiver offsets (Figs. 5a, c, and e) that are related to a single electrical source of the PD array. The symmetric pseudo-sections of the DD array appear in the "without noise" section for all the source-receiver offsets (Figs. 6a, c, and e), whereas the pseudo-sections of the DD array are moderately affected by the presence of noise (Figs. 6b, d, and f), but to a lesser degree compared to the PD array with noise. Since the pseudo-sections show average values of resistivity that are insufficient to show which array is better than the others. Therefore, we performed a 2D inversion to distinguish the advantage and disadvantage between these arrays as shown in Figs. 7 to 9 for the different configurations and the source-receiver offsets. All of the arrays are fitted "without

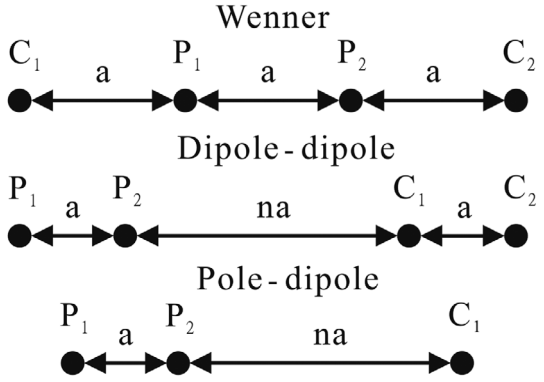

Fig. 2. Illustration of traditional LERI arrays.

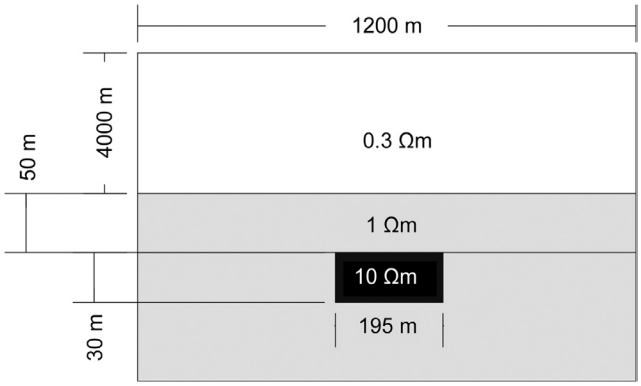

Fig. 3. Initial model in 2D inversion.

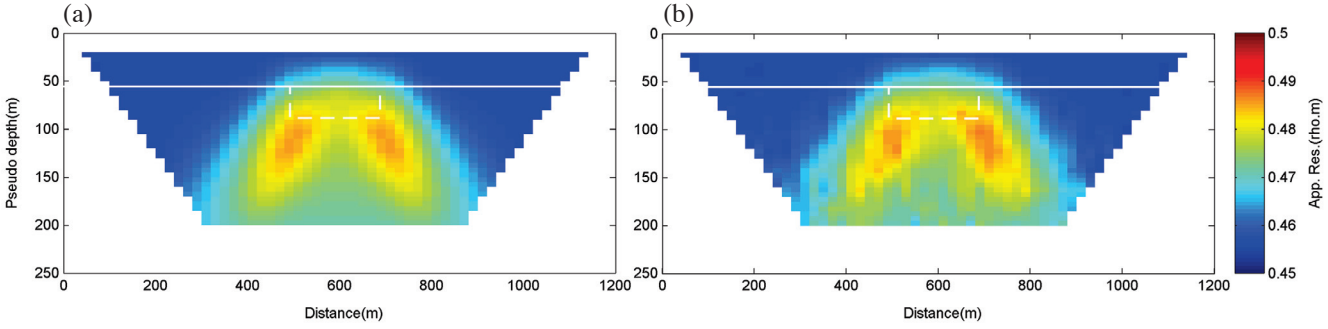

Fig. 4. Pseudo-section of the Wenner array. (a) "Without noise," (b) with 30 μV noise. The white solid line indicates the seafloor and the dotted line shows the MH block.

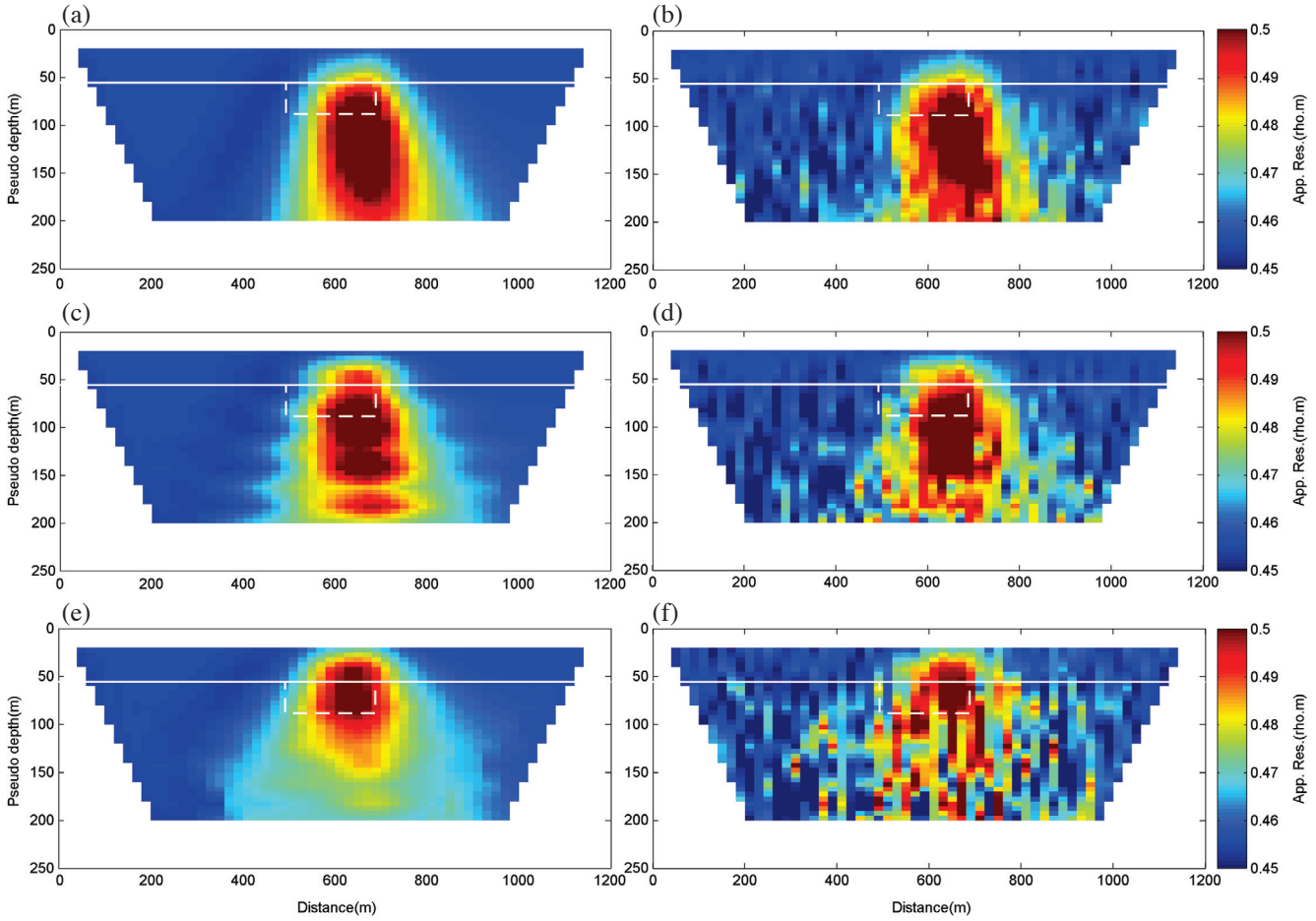

Fig. 5. Pseudo-section of the PD array. (a) Source-receiver offset n = 1 "without noise," and (b) with 30 μV noise. (c) Source-receiver offset n = 1 to 2 "without noise," and (d) with 30 μV noise. (e) Source-receiver offset n = 1 to 3 "without noise," and (f) with 30 μV noise. The white solid line indicates the seafloor and the dotted line shows the MH block.

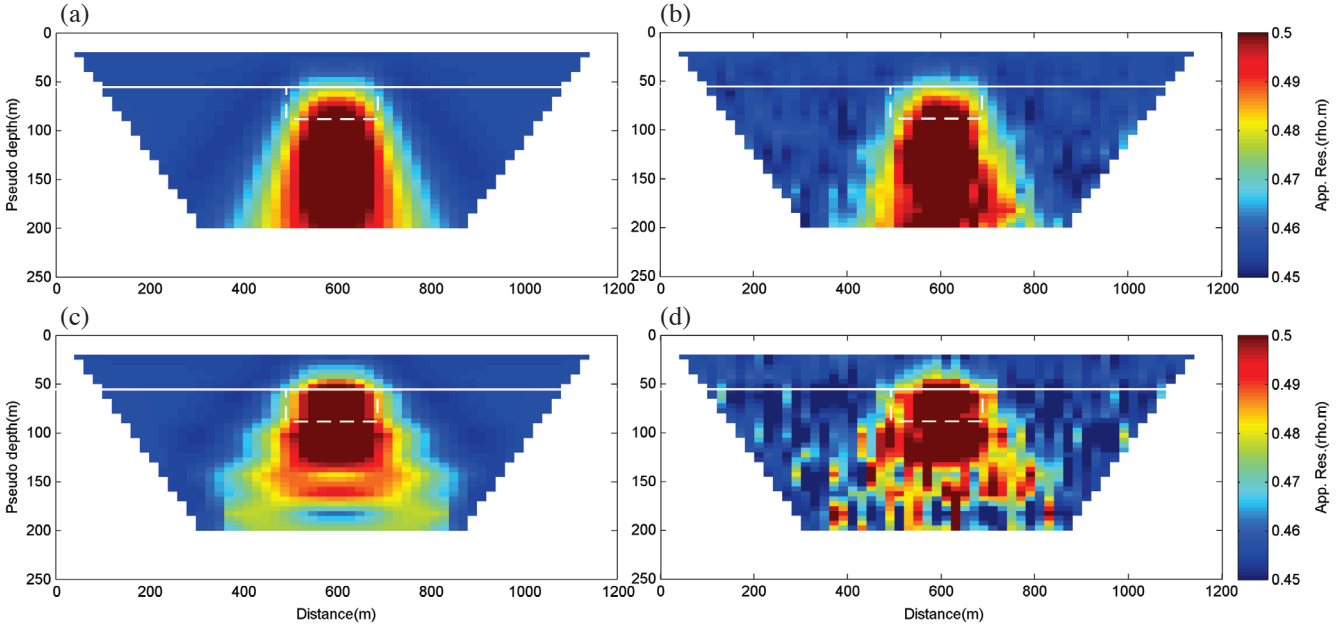

Fig. 6. Pseudo-section of the DD array. (a) Source-receiver offset n = 1 "without noise," and (b) with 30 μV noise. (c) Source-receiver offset n = 1 to 2 "without noise," and (d) with 30 μV noise. (e) Source-receiver offset n = 1 to 3 "without noise," and (f) with 30 μV noise. The white solid line indicates the seafloor and the dotted line shows the MH block.

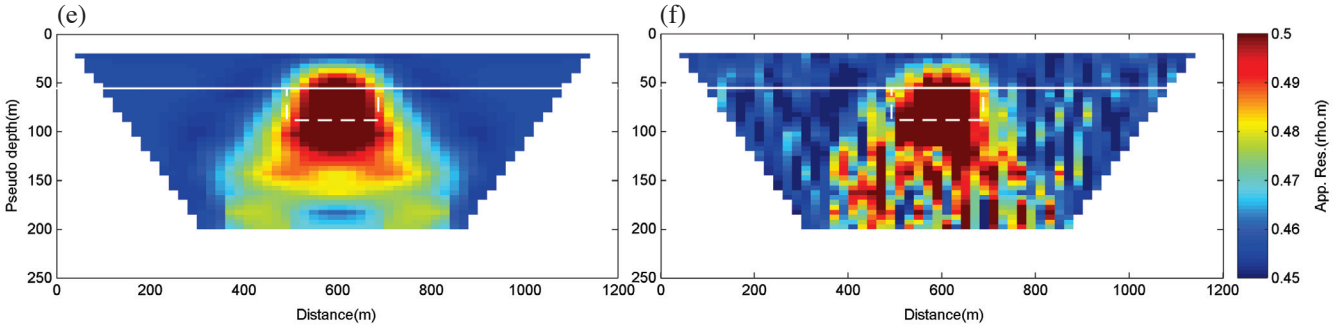

Fig. 6. (Continued)

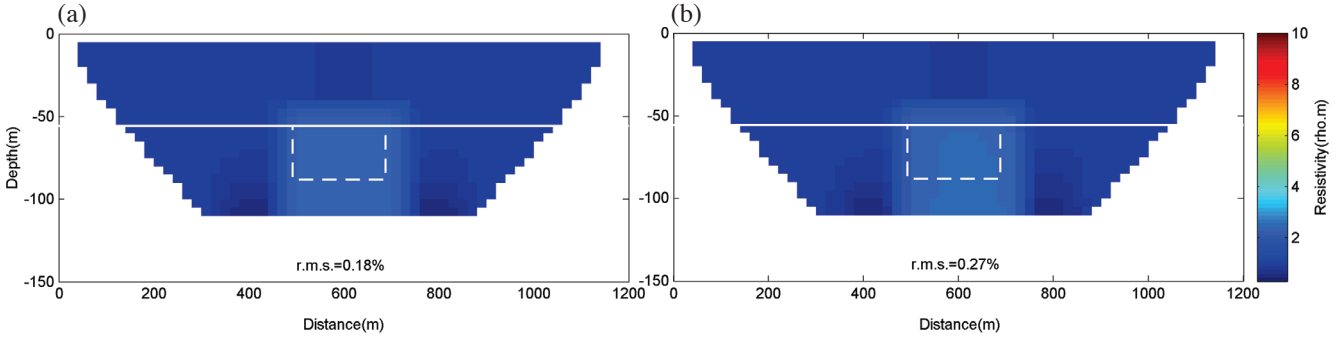

Fig. 7. 2D inversion of the Wenner array. (a) "Without noise," and (b) with 30 μV noise. The white solid line indicates the seafloor and the dotted line shows the MH block.

noise" interference and the root mean square (r.m.s.) misfit is 0.18% for the Wenner array (Fig. 7a), 0.15% - 0.22% for the PD array (Figs. 8a, c, and e), and 0.12% - 0.14% for the DD arrays (Figs. 9a, c, and e). The results from the Wenner, PD, and DD arrays all perform a low r.m.s. misfit of less than 0.3%. The results of adding Gaussian noise to all the arrays are shown in Figs. 7b (Wenner array), 8b, d, and f (PD arrays), 9b, d, and f (DD arrays). These inversions represent significant results both in spatial resolution and resistivity value. The r.m.s. misfit is 0.27% for the Wenner, 0.87% - 2.45% for the PD, and 0.40% - 1.56% for the DD arrays. The r.m.s. misfits increase in long source-receiver offsets for the PD and the DD arrays which indicate that the current amplitude was reduced by large source-receiver offsets and produced large noise levels. Therefore, either selecting a large current amplitude or short source-receiver offset should be required to avoid the noise phenomenon in realistic explorations.

These results indicate that short source-receiver offset (n = 1) provides shallow depth resolution and long source-receiver offsets (n = 1 to 3) images deep structure in the PD and the DD arrays. The PD arrays seem to have a deeper penetration depth than the DD arrays (Figs. 8 and 9), which correspond to the geometric spreading of direct current sounding.

The difference of resistivity anomalies is shown in Table 1. For the source-receiver offset n = 1, the resistivity anomalies of the PD and DD arrays are similar at approximately 3.0 - 3.8 ohm-m, whereas spatial resolution of the DD array is significantly higher than the PD array both with (Figs. 8b and 9b) and "without noise" (Figs. 8a and 9a). For the source-receiver offsets n = 1 to 2, the resistivity anomaly of the PD array is approximately 6.5 ohm-m (Fig. 8c), and the DD array is close to 7.2 ohm-m (Fig. 9c) "without noise;" resistivity of the PD array is approximately 3.6 ohm-m (Fig. 8d) and the DD is approximately 7.0 ohm-m (Fig. 9) with noise. The difference of spatial resistivity anomalies obviously appears with noise data between the two arrays. The MH block (resistivity anomaly) of the PD array is migrated a half size above the seafloor (Fig. 8c), and the DD array (Fig. 9c) also appears similarly, but is slightly less than the PD array. For the source-receiver offsets n = 1 to 3, the resistivity of the PD is approximately 6.0 ohm-m (Fig. 8e) and the DD array is close to 9.0 ohm-m (Fig. 9e) "without noise." The resistivity of the PD array is approximately 5.5 ohm-m (Fig. 8f), and the DD is close to 8.5 ohm-m (Fig. 9f) with noise. The spatial resolution of the DD is higher than that of the PD array. These results indicate that the DD arrays provided the best resolution in the study both with and without noise.

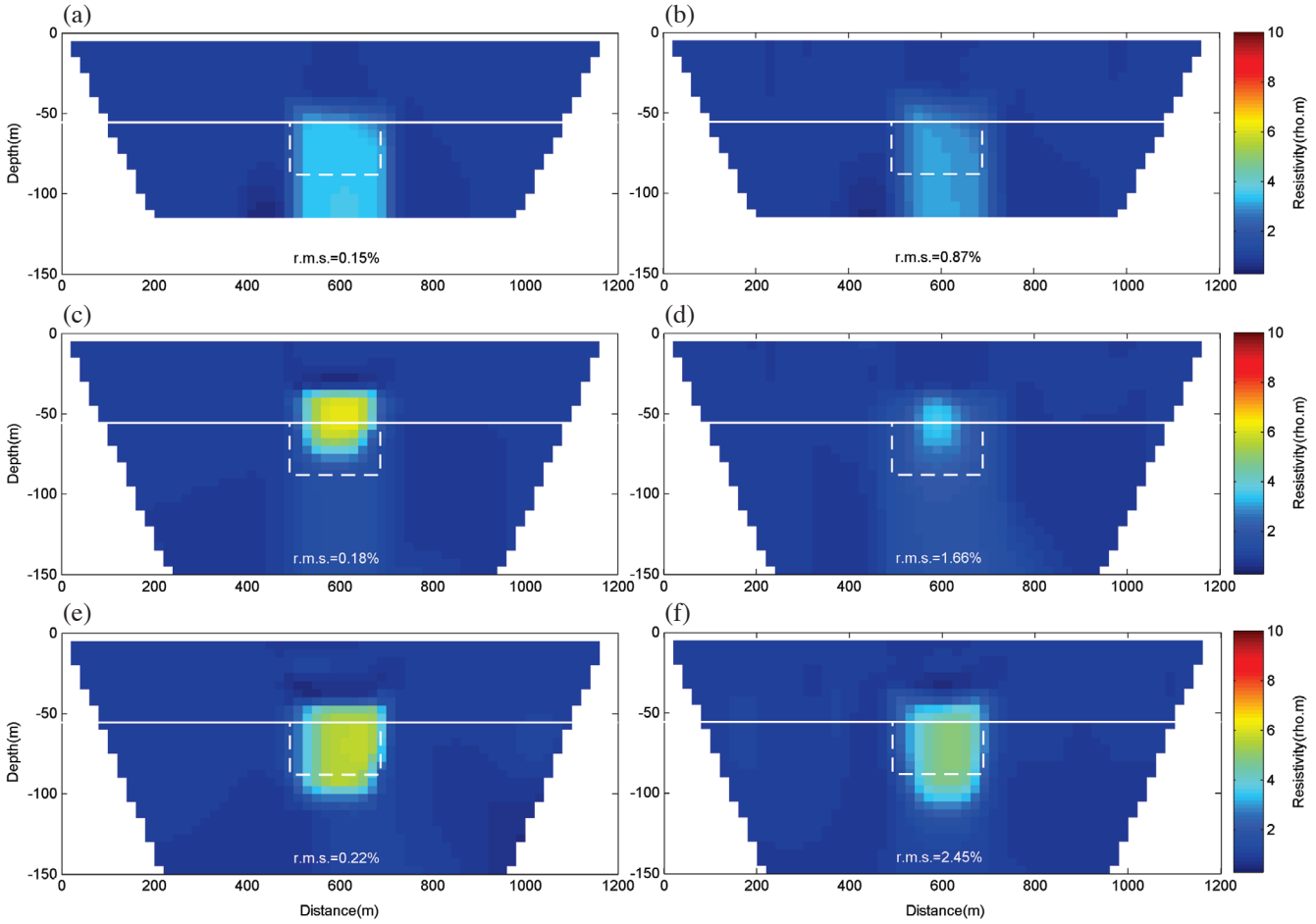

Fig. 8. 2D inversion of the PD array. (a) Source-receiver offset n = 1 "without noise," and (b) with 30 μV noise. (c) Source-receiver offset n = 1 to 2 "without noise," and (d) with 30 μV noise. (e) Source-receiver offset n = 1 to 3 "without noise," and (f) with 30 μV noise. The white solid line indicates the seafloor and the dotted line shows the MH block.

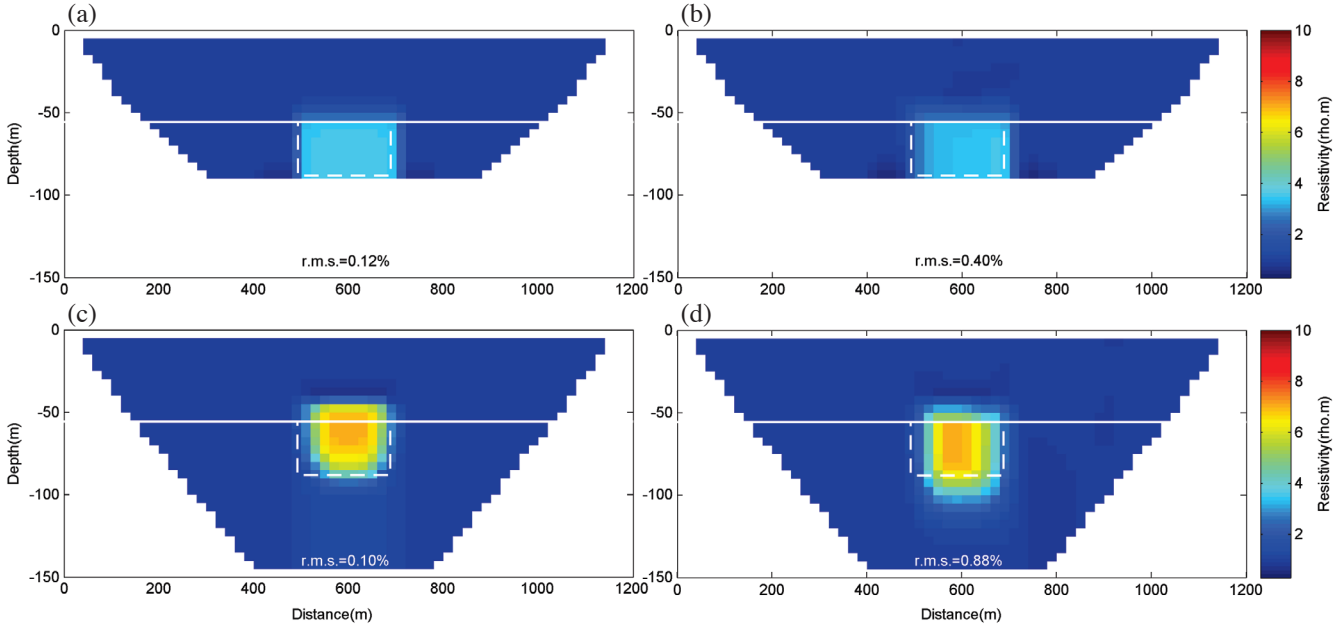

Fig. 9. 2D inversion of the DD array. (a) Source-receiver offset n = 1 "without noise," and (b) with 30 μV noise. (c) Source-receiver offset n = 1 to 2 "without noise," and (d) with 30 μV noise. (e) Source-receiver offset n = 1 to 3 "without noise," and (f) with 30 μV noise. The white solid line indicates the seafloor and the dotted line shows the MH block.

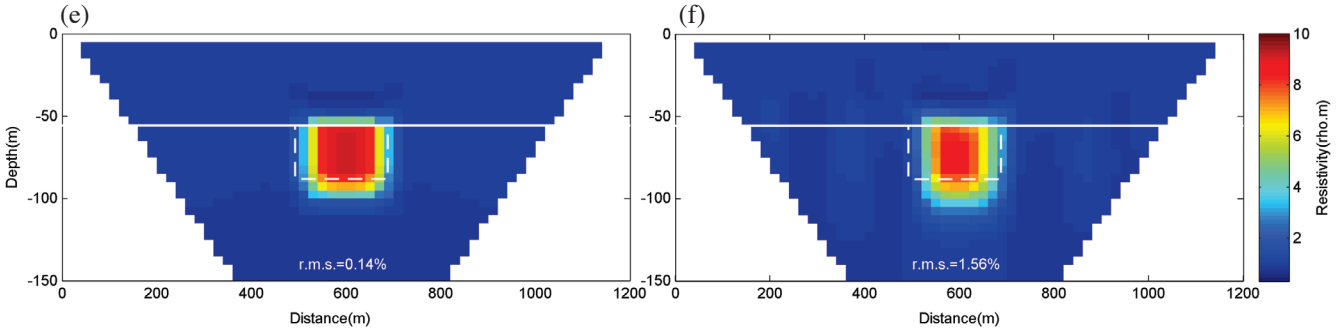

Fig. 9. (Continued)

Table 1. Resistivity anomalies of the PD and DD arrays by 2D inversion.

Source-receiver offset	Arrays	Without noise	Noise
n = 1	PD	3.7 ohm-m	3.8 ohm-m
	DD	3.0 ohm-m	3.5 ohm-m
n = 1 - 2	PD	6.5 ohm-m	3.6 ohm-m
	DD	7.2 ohm-m	7.0 ohm-m
n = 1 - 3	PD	6.0 ohm-m	5.5 ohm-m
	DD	9.0 ohm-m	8.5 ohm-m

4. CONCLUSION

The Wenner array shows the poorest resolution, whereas the PD and DD arrays perform better according to the results. However, realistic MERI exploration is limited by the number of electrodes. Thus, the Wenner array should be eliminated in fields that have a limitation of source-receiver configurations and poor resolution. Changing the source-receiver offsets could greatly improve depth resolution of the PD and the DD arrays, where long offset provides better resolution than short offset both in spatial and resistivity values. Generally, the noise level of MERI is generated by data errors, tides, electrode spacing, altitude, and towed movement, among others. The noise-level range suggested by Goto et al. (2008) is 10% - 15%. Therefore, the authors suggest that static measurement and development receivers on seafloor are required to reduce noise levels.

Acknowledgements The authors would like to acknowledge financial support from the National Science Council of Taiwan under grants No. 97-2917-I-008-104, 100-3113-M-002-001, 100-2914-I-002-057-A1 and 101-2811-M-008-006. We would also like to thank Dr. Edward Bertrand for his patient modifications to our earlier version of the manuscript. This work was partially supported by the Central Geological Survey, MOEA and the Program of Basic Tool Developments for Marine Resource Exploration, funded by the Ministry of Education, Culture, Sports, Science and Technology (MEXT), Japan. We would also like to thank an anonymous reviewer and Dr. Chun-Yi Yu for their constructive comments on the manuscript.

REFERENCES

Chiang, C. W., T. Goto, C. C. Chen, S. K. Hsu, 2011: Efficiency of a marine towed electrical resistivity method. *Terr. Atmos. Ocean. Sci.*, **22**, 443-446, doi: 10.3319/TAO.2011.02.16.01(T). [Link]

Francis, T. J. G., 1985: Resistivity measurements of an ocean floor sulphide mineral deposit from the submersible Cyana. *Mar. Geophys. Res.*, **7**, 419-437, doi: 10.1007/BF00316778. [Link]

Goto, T., T. Kasaya, H. Machiyama, R. Takagi, R. Matsumoto, Y. Okuda, M. Satoh, T. Watanabe, N. Seama, H. Mikada, Y. Sanada, and M. Kinoshita, 2008: A marine deep-towed DC resistivity survey in a methane hydrate area, Japan Sea. *Explor. Geophys.*, **39**, 52-59, doi: 10.1071/EG08003. [Link]

Griffith, D. H. and R. D. Barker, 1993: Two-dimensional resistivity imaging and modelling in areas of complex geology. *J. Appl. Geophys.*, **29**, 211-226, doi: 10.1016/0926-9851(93)90005-J. [Link]

Hyndman, R. D., J. P. Foucher, M. Yamano, A. Fisher, and Scientific Team of Ocean Drilling Program Leg 131, 1992: Deep sea bottom-simulating-reflectors: Calibration of the base of the hydrate stability field as used for heat flow estimates. *Earth Planet. Sci. Lett.*, **109**, 289-301, doi: 10.1016/0012-821X(92)90093-B. [Link]

Johnson, A. H. and M. D. Max, 2006: The path to commercial hydrate gas production. *The Leading Edge*, **25**, 648-651, doi: 10.1190/1.2202672. [Link]

Kvenvolden, K. A., 1988: Methane hydrates and global climate. *Global Biogeochem. Cycles*, **2**, 211-229, doi: 10.1029/GB002i003p00221. [Link]

Lin, S., W. C. Hsieh, Y. C. Lim, T. F. Yang, C. S. Liu, and Y. Wang, 2006: Methane migration and its influence on sulfate reduction in the good Weather Ridge region, South China Sea continental margin sediments. *Terr.*

Atmos. Ocean. Sci., **17**, 883-902.

Loke, M. H. and R. D. Barker, 1996: Rapid least-squares inversion of apparent resistivity pseudosections by a quasi-Newton method. *Geophys. Prospect.*, **44**, 131-152, doi: 10.1111/j.1365-2478.1996.tb00142.x. [Link]

Paull, C. K., R. Matsumoto, P. J. Wallace, and W. P. Dillon, 2000: Proceedings of the Ocean Drilling Program - Scientific Results, 164.

Schwalenberg, K., M. Haeckel, J. Poort, and M. Jegen, 2010: Evaluation of gas hydrate deposits in an active seep area using marine controlled source electromagnetics: Results from Opouawe Bank, Hikurangi Margin, New Zealand. *Mar. Geol.*, **272**, 79-88, doi: 10.1016/j.margeo.2009.07.006. [Link]

Shipley, T. H., M. H. Houston, R. T. Buffler, F. J. Shaub, K. J. McMillen, J. W. Ladd, and J. L. Worzel, 1979: Seismic evidence for widespread possible gas hydrate horizons on continental slopes and rises. *AAPG Bull.*, **63**, 2204-2213, doi: 10.1306/2F91890A-16CE-11D7-8645000102C1865D. [Link]

Thirud, A. P., 2002: EMGS article: Scandinavian Oil-gas Magazine 3/4, 8-9.

Von Herzen, R. P., J. Kirklin, and K. Becker, 1996: Geoelectrical measurements at the TAG Hydrothermal Mound. *Geophys. Res. Lett.*, **23**, 3451-3454, doi: 10.1029/96GL02077. [Link]